The influence of stress on the oxidation of a ni-based superalloy

Taylor, Mary; Evans, Hugh; Ramsay, Joshua; Child, Danial; Hardy, Mark

DOI:
10.1016/j.corsci.2019.04.023

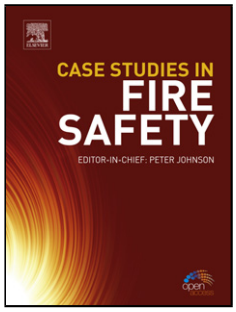

Title: THE INFLUENCE OF STRESS ON THE OXIDATION OF A Ni-BASED SUPERALLOY

Authors: J.D. Ramsay, H.E. Evans, D.J. Child, M.P. Taylor, M.C. Hardy

PII: S0010-938X(19)30375-0
DOI: https://doi.org/10.1016/j.corsci.2019.04.023
Reference: CS 7989

To appear in:

Received date: 22 February 2019
Revised date: 17 April 2019
Accepted date: 19 April 2019

Please cite this article as: Ramsay JD, Evans HE, Child DJ, Taylor MP, Hardy MC, THE INFLUENCE OF STRESS ON THE OXIDATION OF A Ni-BASED SUPERALLOY, *Corrosion Science* (2019), https://doi.org/10.1016/j.corsci.2019.04.023

THE INFLUENCE OF STRESS ON THE OXIDATION OF A Ni-BASED SUPERALLOY

J.D. Ramsay[1], H.E. Evans[1], D.J. Child[2], M.P. Taylor[1*] and M.C. Hardy[2].

[1] School of Metallurgy and Materials, University of Birmingham, Birmingham, B15 2TT, UK.
[2] Rolls-Royce, PO Box 31, Derby, DE24 8BJ, UK.

* Corresponding author: m.p.taylor@bham.ac.uk

HIGHLIGHTS

- External chromia thickness was unaffected by stress.
- Tensile stress resulted in increase of alumina penetration by factor of 2.
- This is taken to be evidence of Stress Aided Grain Boundary Oxidation (SAGBO).
- Tensile stress at the tip of the intrusion increases the anion vacancy concentration.
- Leads to flux of oxygen vacancies along intrusion, increasing the growth rate.

ABSTRACT
Double edge notched specimens of the Ni-based superalloy RR1000 have been subjected to 1-1-1-1 fatigue tests with R=0 at 750°C in air for 111 hours at a peak elastic stress of 900 MPa. Extensive measurements of the thickness of the chromia layer formed during this exposure period show no influence of the applied stress. In contrast, the depth of the intergranular alumina penetrations underlying the chromia layer were approximately a factor of 2 larger in the most stressed regions (base of the notches) than in unstressed regions adjacent to the notches. This difference was highly significant and is considered to demonstrate Stress Aided Grain Boundary Oxidation (SAGBO). A model for this process has been developed in which the tensile stress at the tip of the alumina intrusion increased the anion vacancy concentration there and the vacancy flux along the intrusion. A consequence was that the intrusion growth rate increased above that in the absence of stress. The observed increase of a factor of 2 in intrusion length is estimated to be achievable at a tensile stress of ~1 GPa within the intrusion at its tip. This is considered to be plausible in such a high-strength alloy.

Key Words: Fatigue; Ni-based Superalloys; Oxidation; Alumina; Stress-Aided Grain Boundary Oxidation (SAGBO).

1. INTRODUCTION

It is now well recognised that stress, whether applied, thermal or induced by oxide growth, can affect the oxidation of metals and alloys [1-6]. Studies to date have tended to focus on the behaviour of surface oxide layers and have supported the expectation [7] that tensile stress may induce oxide cracking whereas compressive stress may initiate oxide spallation either through a buckling or wedging process. In either case, the damage to the surface oxide, which provided protection, results in an increase in the rate of oxidation [5,8-10].

For those oxides, e.g. ZrO_2 or Al_2O_3 that form new oxide at the base of the surface layer, significant compressive growth stress have been measured within the oxide layer [11-13] reaching values as high as ~1 GPa. It has been suggested [14] that such values are sufficiently high to have a measurable influence on the thermodynamics of anion vacancy formation at the oxide/metal interface and could explain the sub-parabolic growth kinetics of ZrO_2 on Zircaloy. The concept has also been applied by Limarga and Wilkinson [15,16] to the nitridation of TiAl exposed to 4-point bending. They confirmed that tensile stress increased the rate of penetration of the nitride front whereas compressive stress reduced it. Their results were well described by an expression of the form of Equation (1), which derives from the earlier theoretical treatment [14,17]:

$$\frac{dy}{dt} = \frac{D_i}{y} \exp\left(\frac{\sigma_H \Delta\Omega}{kT}\right) \qquad (1)$$

Here, y is the thickness of the nitride layer, dy/dt the rate of thickening of the layer, D_i is the diffusion coefficient, $\Delta\Omega$ is the volume change increase (positive) on converting TiAl to TiN, σ_H is the local hydrostatic stress (positive when tensile), k is Boltzmann's constant and T is absolute temperature. A similar formulation has been used in other modelling studies of mechanical/oxidation interactions on the growth of the surface oxide layer [18-23].

High temperature alloys have compositions that are intended to form a protective oxide layer, usually chromia or alumina. Important classes of such alloys are chromia-forming stainless steels and Ni-based superalloys. However, these alloys also contain elements, in particular Al,

Ti and Si, which form oxides that are more thermodynamically stable than chromia. As a result, internal oxidation of these elements can form and often does so as intergranular intrusions of silica in the stainless steels [24] or of alumina in the chromia-forming Ni-based superalloys [25-27]. This is a significant form of environmental degradation because fatigue cracks are known [28] to nucleate at alumina intrusions in the RR1000 superalloy used for aero-engine turbine discs. It is important to know whether the growth rate of such intrusions can be affected by imposed stress, i.e. whether Stress Aided Grain Boundary Oxidation (SAGBO) can occur.

The earliest mention of SAGBO has been traced back to 1980 [29], but it is possible it was first proposed some years before. Since then, it has proven elusive to demonstrate experimentally that the phenomenon occurs. The focus has been on crack propagation, typically under fatigue conditions, in an oxidising environment at high temperatures where accelerated crack growth occurs [30-34]. The term "SAGBO" has been used occasionally to describe this process [31,35-42] but two distinctly different mechanisms have been postulated. Under the category of dynamic embrittlement, stress-aided diffusion of elemental oxygen is envisaged to occur along the alloy grain boundary ahead of the crack tip. Its presence there is thought to reduce the cohesive strength of the grain boundary and, in so doing, produce conditions for an increased rate of crack propagation. Whereas long-range intergranular diffusion of elemental oxygen is known to occur [43] in Ni under test conditions in which internal oxidation only of carbon was possible, it is implausible in typical commercial alloys [44]. Such alloys contain elements with high affinity for oxygen (e.g. Cr, Al, Ti, Si) and these can be expected to getter elemental oxygen at the crack tip to form oxide phases. Intergranular oxidation ahead of fatigue cracks in Udimet 500 was reported decades ago by McMahon [45] but was attributed to long-range diffusion of oxygen and oxidation of Cr-rich carbide precipitates, i.e. a variant of dynamic embrittlement. Recent TEM studies on alloy 718 [35][46], Udimet 720Li [47], and RR1000 [44],[48], indicate that intergranular oxidation emanates from the crack tip to form an intergranular oxide intrusion which contains oxide layers of Co, Ni, Cr, Ti and Al arranged in the order of their thermodynamic stability. In addition, atom probe tomography [36][49] and nanoSIMS [36],[47],[50] studies failed to detect elemental oxygen ahead of these oxide intrusions, consistent with their high thermodynamic stability. These recent observations provide persuasive evidence that the damaging effect of an oxidising environment arises from the fracture of these brittle oxides which will lead to enhanced crack growth. SAGBO, however, would also require the intrusion growth rate along the grain boundary to be increased by tensile stress, a detail seldom reported since the term was coined [51-54].

In recent TEM observations [44], it was suspected that an enhanced rate of growth of the oxide intrusion ahead of a fatigue crack in the Ni-based superalloy RR1000 had indeed taken place. A new SAGBO model was suggested [55] to account for these observations based on the principle that the anticipated tensile stress at the tip of the intrusion would increase the anion vacancy flux to the crack tip and, hence, the growth rate of the intrusion. The underlying concept is the same as that suggested previously [14] to account for sub-parabolic zirconia growth. Using the equivalent of equation (1), the estimated enhancement factors for the oxide intrusions in RR1000 were found [55] to be commensurate with the presence of an intrusion tip stress of around 1 GPa which was considered not unreasonable for the alloy. Whereas these initial results were encouraging, it is recognised that they derive from complex circumstances, in which cracks and multiple oxide types were present, and need to be treated with some caution.

The purpose of the present work was to explore the SAGBO concept further but using a simpler experimental arrangement in which a single oxide is examined in the absence of a crack. The Ni-based RR1000 alloy was again used because such high-strength alloys can sustain the high intrusion stresses (~ 1GPa) thought to be needed to produce measurable changes in oxidation behaviour. In common with other chromia-forming superalloys [25], intergranular intrusions of alumina develop [27] beneath the surface oxide and it is the growth of these that is considered in the present work.

2. EXPERIMENTAL METHOD

The nominal composition of the RR1000 alloy used in this study is given in Table 1. The alloy, produced by powder metallurgy, was supplied by Rolls-Royce as machined and shot-peened specimens of double-edge notched (DEN) configuration, as shown in Figure 1. The average grain size was ~40 μm.

Table 1: Nominal composition of RR1000 in both weight and atomic %

	Ni	Co	Cr	Mo	Ti	Al	Ta	Hf	Zr	C	B
Weight %	bal.	18.5	15.0	5.0	3.6	3.0	2.0	0.5	0.06	0.02	0.03
Atomic %	bal.	17.9	16.5	3.0	4.3	6.4	0.6	0.2	0.04	0.14	0.10

These specimens were subjected to fatigue loading at 750°C in air under a conventional R=0 trapezoidal 1-1-1-1 waveform, i.e. 1 second from zero to maximum tensile stress, a hold at the maximum for 1 second, followed by a reduction to zero in 1 second and a hold there for 1 second, and the sequence is repeated. In the present tests, each 4-second cycle was applied ~100,000 times, i.e. equivalent to a test time of ~111 hours. The maximum applied stress in these cycles was designed to produce an estimated tensile peak stress at the base of the notches of 900 MPa. Fatigue testing under these conditions did not result in specimen failure nor crack development nor oxide cracking.

After testing, the mid-section of the sample, containing the notches, was sectioned, sputtered with gold and plated with nickel. It was then mounted in a conductive Bakelite resin and ground using progressively finer grades of wet SiC papers before being polished with progressively finer diamond solutions. The final polish was performed using OP-S colloidal silica solution.

Examination was performed on the cross sections using a Jeol 7000F Field Emission Gun (FEG) Scanning Electron Microscope (SEM), fitted with Energy Dispersive Spectroscopy (EDS) used with an acceleration voltage of 20 kV. Images were taken at three different locations, denoted A, B, C on each notch of the samples as shown in Figure 1. Location B experiences the highest value of axial applied stress (900 MPa) whereas at locations A and C, the applied stress, both axial and tangential, will approximate to zero because of the proximity of the free surfaces. This has been confirmed by finite element analysis (L. Kovacs, Rolls-Royce, unpublished work).

At least four sets of five measurements of the external chromia thickness and internal oxide penetration depths were taken from each location over a length of ~80 µm using backscattered electron (BSE) images and Image J 1.48 analysis software. Approximately 120 µm was then removed from the cross section thickness by further polishing to expose a further set of grains for which the surface oxide thickness and intergranular penetration depths were measured. This procedure yielded a total of 40-50 measurements per location for each notch.

3. RESULTS

3.1 Surface Oxide

Consistent with previous work [56], the surface oxide consisted of a titanium-enriched chromia layer, with an outer layer of discontinuous rutile, together with internally growing alumina intrusions within the alloy matrix, Figure 2 and Table 2. The internal intrusions are described

as intergranular, because formation predominantly occurs at the grain boundaries of small recrystallized grains with a diameter of approximately 1-3 μm, Figure 2, also described in [56]. In Figure 2, two images from the same section are included with different contrast settings, used here to emphasise the presence of recrystallized grains. This general morphology was present at the locations (B) experiencing the maximum applied stress and at those (A, C) with negligible applied stress. A set of EDS point scans down one of these intrusions is shown in Figure 2, together with results for each point in Table 2. The results from points 3 and 4 are expected to be an underestimate of the aluminium content of the intrusion as, due to the size of the interaction volume of the electron beam (having a diameter of 1 μm and an estimated depth of no more than 1.1 μm), X-rays from the intrusion and the surrounding depleted alloy will contribute to the signal. Therefore, the results indicate the intrusions are alumina.

The chromia layer thicknesses measured for each of the sampling locations are shown as the cumulative probability plots of Figure 3. A normal distribution has been used to describe the data. Figure 3(a) gives the results for locations A_1, B_1 and C_1 and Figure 3(b) those for locations A_2, B_2 and C_2.

Clearly, differences exist between the distributions, even at the 95% confidence level. It is thought that these originate from occasional delamination of the Ni plate from the A and C locations during specimen preparation. It is likely that this results in some loss of oxide also and this will lead to smaller measured oxide thickness values at these locations. This is particularly evident for Notch 2 (Figure 3b) where the measured oxide thickness at Location C is consistently less than at Location A, the other unstressed location. The important feature of the results, however, is that there does not appear to be a significant difference between the mean oxide thickness values in stressed (Location B) and unstressed regions when delamination did not occur.

It is difficult to estimate the stress in the external oxide during formation at the stressed location B, as the net stress is complicated by stresses associated with the growth of the oxide. During the unloaded part of the fatigue cycle it is likely that the oxide is in compression. The strain experienced by the oxide, however, will be that imposed by the elastic strain occurring in the test piece. Assuming a stress of 900 MPa at the base of the notch and a Young's modulus of 150 GPa for this alloy at the test temperature of 750°C, this equates to a maximum strain of approximately 6×10^{-3}. The wave form used in this test dictates that this strain is applied during the 1s loading ramp, imposing a strain rate of 6×10^{-3} s^{-1}, followed by a 1s hold before unloading. At this strain rate and temperature, it has been shown that through thickness

cracking of chromia formed on flat test specimens occurs under tensile stresses [57]. At the strain rate imposed in this work, cracking at intervals of ~25-30 μm would be expected. The sections at the base of the notch under examination were ~80 μm and thus if this were the case, one to three uniformly spaced cracks would be expected to have formed. This would result in highly localised changes to oxide thickness and impact the internal oxidation of the alloy. However, if the oxide is growing under compression the net tensile stress will be proportionally reduced and thus, although the strain rate is fast enough to crack the surface oxide the maximum strain level is not sufficiently high.

It can then be inferred that the growth of the surface oxide layer is not affected significantly by the loading conditions. This indicates that the applied stress has negligible effect on the ionic transport through the oxide layer but this is not unexpected because, unlike the case of zirconia [14] or alumina, the dominant diffusing species is the cation. It means that new oxide is formed on the outer surface of the oxide layer where the volume expansion can occur into free space. Of significance, particularly for the present work, is that the measurements show no evidence of cracking or spallation of the surface oxide in the region of maximum applied stress (location B) since this would lead to an enhanced oxide growth rate locally, as described above, but this was not observed. This can be appreciated further from the cross-sections shown in Figure 4 which also demonstrate the insensitivity of the surface-oxide thickness and morphology to the presence of an applied stress.

3.2 Intergranular Oxidation

As can be seen from Figures 2 and 4, intergranular intrusions form underneath the surface oxide layer. These consist of alumina and are a characteristic feature of such chromia-forming superalloys [25-27]. Figure 4 compares, for each notch, the microstructure at the most highly stressed region (Location B) with that at which the applied stress is approximately zero (Location C, for the examples shown). It is striking that the penetration depth at Location B, for both notches, is appreciably greater than at Location C. This difference was quantified in the same way as used for the surface oxide thickness, i.e. cumulative probability plots were produced from approximately 45 measurements for each of the six sampling locations. The penetration quoted is measured from the base of the surface oxide layer to the tip of the alumina intrusion. In this case, the measurements were unaffected by any delamination of the outer regions of the surface oxide during sample preparation.

The cumulative probability plots of Figure 5 show that there are no significant differences in penetration depths at Locations A and C for each of the two notches or between the notches as can be appreciated from the overlapping of the 95% confidence limits. In contrast, the penetration depths in both highly-stressed notch roots (Locations B) are greater than in Locations A and C to a high degree of significance. This difference is clear from Figure 4. It is also evident from Figure 5 that the notch penetrations differ significantly between notches with Notch 2 exhibiting larger depths (compare Figures 4(a) and 4(b)).

The penetration depths for Notch 1, as determined by the 50% cumulative probability values, are 1.19 µm for Location 1A and a similar value of 1.30 µm for Location 1C. Location 1B, on the other hand, shows a penetration depth of 2.33 µm. The ratio of penetration depths for Location 1B with the average for Locations 1A and 1C provides an *enhancement factor*, S_ℓ , which will be used as part of the theoretical development later in the paper. The value of S_ℓ for Notch 1 is 1.9 and that for Notch 2 is 2.5 based on the cumulative probability plots of Figure 5. The difference in enhancement factor between the two notches may be due to a difference in the extent of shot peening, applied manually to the test piece, but the situation is unclear at this time. The values are consistent with the images shown in Figure 4 and it is considered that the observations demonstrate the presence of Stress-Aided Grain Boundary Oxidation (SAGBO) in these tests. The next section of the paper will develop a model for SAGBO and its viability in explaining these deduced enhancement factors will be assessed in the Discussion.

4. THE PROPOSED SAGBO MECHANISM

The growth of the alumina intrusion requires oxygen to diffuse through the surface layer of chromia and along the intrusion to its tip where new oxide is formed. In each case, transport is expected to be via short-circuit diffusion paths, predominantly grain boundaries, but the rate of growth of the intrusion could, in principle, be determined by diffusion through the chromia layer or along the alumina intrusion. It will be assumed here that the latter is rate determining.

Oxygen diffusion is expected to occur by exchange with oxygen vacancies and it is the concentration gradient of these vacancies along the length of the intrusion that determines its rate of growth. Oxygen vacancies are created at the intrusion tip as a consequence of the formation of new alumina and the extension of the intrusion. The process is shown schematically in Figure 6. The defect structure of alumina is not well established and, for

present purposes, the ions and vacancies are assumed to be neutrally charged; this assumption has no significant influence on the development of the model. The reaction that occurs at the tip of the intrusion is:

$$2Al + 3O \longrightarrow Al_2O_3 + 3V \qquad (A)$$

Here O is an oxygen ion on the anion sub-lattice in alumina and V is a corresponding oxygen vacancy. An overall change in volume, $\Delta\Omega$, is associated with this reaction:

$$\Delta\Omega = (\Omega_{Al2O3} - 2\Omega_{Al}) - 3(\Omega_O - \Omega_V) = \Omega_A - 3\Omega_B \qquad (2)$$

Here, Ω represents the volume of the particular species, A is the first bracketed term and B the second. Although the vacancy volume is unknown, it is expected that Ω_B will be much smaller than the volume change, Ω_A, produced on formation of the oxide so that the volume change associated with reaction (A) can be approximated as:

$$\Delta\Omega \sim (\Omega_{Al2O3} - 2\Omega_{Al}) = \Omega_A \qquad (3)$$

This volume change is substantial and estimated in the Appendix as a 93% volume expansion. In an isotropic solid, this strain would be distributed uniformly in the three principal directions. In the present case, however, the oxide is being formed along the plane of a grain boundary and it seems intuitively reasonable to assume that the dilatational strain manifests perpendicular to this plane. The expansion results in reactive stresses that are compressive along at least part of the length of the intrusion [55] but which become tensile at the intrusion tip. Two possible examples are shown in Figure 7 which represent different intrusion morphologies in Figure 4. For a wedge-shaped intrusion (Figure 7(a)), the compressive stress is largest near the surface oxide layer but diminishes with distance along the intrusion length, becoming tensile towards the tip if continuity across the oxide/metal interface is to be maintained. For the parallel-sided intrusion of Figure 7(b), the stress remains compressive along its length except at its tip where a thinner, curved region of new oxide would be expected to form.

Stress will affect the diffusion of vacancies along the intrusion in two ways, implicit in equation (4):

$$\left(J_v\right)_\sigma = -D_v \left\{ \frac{\partial C_v}{\partial x} - \frac{C_v \Omega_B}{kT} \frac{\partial \sigma}{\partial x} \right\} \qquad (4)$$

Here, $(J_v)_\sigma$ is the vacancy flux in the presence of stress, C_v is the vacancy concentration and D_v is the vacancy diffusion coefficient.

The second term in the brackets in equation (4) reflects the drift imposed by a stress gradient along the intrusion. For the case of the planar intrusion, Figure 7(b), the gradient should be negligible and there will be no drift term. For the wedge-shaped intrusion there will be a stress gradient, as shown schematically in Figure 7(a), and this will act on the volume change Ω_B, the difference in volume between an oxygen atom and its vacancy. This is taken to be small and negligible because diffusion is occurring substitutionally. If it was occurring by interstitial transport then the volume term would correspond to the expansion caused by the interstitial and would not be negligible. For the present case, equation (4) simplifies to:

$$J_v = -D_v \frac{\partial C_v}{\partial x} \qquad (5)$$

The local stress, σ, also affects the boundary conditions for vacancy concentration through its effect on the vacancy chemical potential. It results in a modified vacancy concentration given by [14,17]:

$$C_v = C_o \exp \frac{\sigma \Omega_A}{kT} \qquad (6)$$

The subsequent model development follows that used to predict growth rates of an oxide intrusion ahead of a crack but is included here for completeness. Equation (6) is used to define the diffusion boundary conditions, i.e. the vacancy concentration, $(C_v)_{it}$ at the tip of the intrusion and also that, $(C_v)_{ib}$ at its base where it joins the surface oxide layer. These concentrations differ and lead to a concentration gradient along the intrusion length, ℓ, to give the vacancy flux $(J_v)_\sigma$ in the presence of stress as:

$$(J_v)_\sigma \propto \frac{D_v}{\ell}\left[(C_v)_{it} \exp\left(\frac{\sigma_{it}\,\Omega_A}{kT}\right) - (C_v)_{ib} \exp\left(\frac{\sigma_{ib}\,\Omega_A}{kT}\right)\right] \qquad (7)$$

The oxygen vacancy concentration at the tip of the intrusion is obviously larger than that at its base, otherwise O could not diffuse down its length in the counter flux of vacancies and allow the intrusion to grow even in the absence of stress. In fact, it is expected that $(C_v)_{it} >> (C_v)_{ib}$ commensurate with the much smaller oxygen activity at the tip of the intrusion than at its base.

Additionally, the role of stress will be to increase this difference because of the tensile conditions at the intrusion tip but compressive at its base. The reasonable assumption is then that the second term in the square bracket of equation (7) will be much smaller than the first and may be neglected. Noting also that the rate of growth of the intrusion is proportional to the vacancy flux, this stress-affected rate can then be approximated as:

$$\left(\dot{\ell}\right)_{\sigma} = K\left(J_v\right)_{\sigma} = \frac{KD_v\left(C_v\right)_{it}}{\ell}\exp\left(\frac{\sigma_{it}\,\Omega_A}{kT}\right) \tag{8}$$

This is essentially of the same form as equation 1. K is a constant that allows for the increase in intrusion size per O atom that emerges at the tip and is insensitive to the presence or absence of stress. The ratio, S_r, of growth rates in the stressed to unstressed state, $\sigma_{it}=0$, can then be used as a measure of the SAGBO effect at a given intrusion length, ℓ.

$$S_r = \left[\frac{\left(\dot{\ell}\right)_{\sigma}}{\left(\dot{\ell}\right)_{o}}\right]_{\ell} = \exp\frac{\sigma_{it}\,\Omega_A}{kT} \tag{9}$$

5. DISCUSSION

The main purpose of this Discussion is to assess whether the SAGBO model described above can explain the observed results of enhanced intergranular penetration in stressed regions at plausible values of the intrusion tip stress, σ_{it}. The evidence and explanation provided earlier discounts surface oxide cracking as a potential mechanism. The parameter S_r of equation (9) gives the ratio of intrusion growth rates with and without stress for a given intrusion length, ℓ. The current tests have determined the stress effect on intrusion length rather than on its rate of growth and consideration now needs to be given to the integration of equation (8) to give intrusion length.

For the case that σ_{it} is invariant with both exposure time and intrusion length, equation (8) is readily integrated as:

$$\int_0^{\ell} \ell \, d\ell = KD_v \left(C_v\right)_{it} \exp\left(\frac{\sigma_{it}\,\Omega_A}{kT}\right) \int_0^{t} dt \tag{10}$$

to give the parabolic rate equation:

$$\left(\ell_\sigma\right) = \left[2KD_v \left(C_v\right)_{it} \exp\left(\frac{\sigma_{it}\,\Omega_A}{kT}\right)\right]^{0.5} t^{0.5} \tag{11}$$

If σ_{it} were to vary with ℓ and t, equation (11) would be modified and parabolic kinetics would be unlikely to occur. This aspect is presently unresolved but helpful insights can be obtained from the work by Cruchley et al. [27] who showed that parabolic intergranular oxidation kinetics occurred in this alloy, albeit tested in the absence of an applied stress.

The stress, σ_{it}, in equation (11) acts orthogonally to the plane of the grain boundary at the tip of the alumina intrusion and within that intrusion. Linear elastic conditions are then expected to apply. Three contributors to this stress can be identified and these may be superimposed:

$$\sigma_{it} = \sigma_{ox} + \sigma_{sp} + \sigma_{ap} \tag{12}$$

Here, σ_{ox}, is the stress generated within the intrusion by the dilatational strain produced on formation of the intrusion (Figure 7). Its magnitude will vary with the intrusion shape but it will be tensile at the intrusion tip. The component σ_{sp} is the stress generated by the shot-peening operation. σ_{ap} is the stress generated within the intrusion at its tip by the applied load. It will be tensile in the present tests with an expected magnitude between the applied stress and the fracture stress of the alumina intrusion. It will vary through the fatigue cycle in the same manner as the applied load.

The contributions made by σ_{ox} and σ_{sp} to the intrusion tip stress were present at similar magnitude in Cruchley's tests [27]. Parabolic kinetics were still found, however, indicating that neither parameter, nor their algebraic sum, varied significantly with intrusion length or exposure time. The dependence of σ_{ap} is less clear but, to a first approximation, it will be assumed that it also is insensitive to these parameters. Equation (12) is now used in equation (11) to isolate the contribution of σ_{ap}:

$$\left(\ell_\sigma\right) = \left[2KD_v \left(C_v\right)_{it} \exp\left(\frac{(\sigma_{ox} + \sigma_{sp})\Omega_A}{kT}\right) \exp\left(\frac{\sigma_{ap}\,\Omega_A}{kT}\right)\right]^{0.5} t^{0.5} \tag{13}$$

Equation (13), with σ_{ap}=0, reduces to that describing the kinetics of intergranular oxidation in regions of the specimen free of applied stress, i.e. Locations A and C shown in Figure 1. This allows a SAGBO parameter, S_ℓ, in terms of intrusion length at a given exposure time, to be defined as the ratio of equation (13) evaluated with $\sigma_{ap} \neq 0$ to that with $\sigma_{ap} = 0$:

$$S_\ell = \left(\frac{\ell_\sigma}{\ell_0}\right)_t = \exp\left(\frac{\sigma_{ap}\,\Omega_A}{2kT}\right) \tag{14}$$

Here, ℓ_σ is the intrusion length at a given time in the presence of an applied stress (Location B in Figure 1) and ℓ_0 is the corresponding value in the absence of an applied stress (Locations A and C). The variation of S_ℓ with σ_{ap}, calculated using Ω_A = 2.07x10^{-29} m^3 (Appendix), k = 1.38x10^{-23} J.K^{-1} and T = 1023 K, is shown in Figure 8.

The values for S_ℓ found in the present work ranged from 1.9 for Notch 1 to 2.5 for Notch 2 (Figures 4 and 5) and this range is shown as the horizontal shaded area in Figure 8. The corresponding predicted tensile stresses (equation 14) in the alumina intrusion at its tip are shown as the vertical shaded area in Figure 8 ranging from ~875 to ~1250 MPa. These stresses represent an effective average value through the course of the fatigue cycle since the enhancement factors measured also represent an average value. The stresses are high but not excessively so for this high-strength superalloy and seem plausible. The peak section stress of 900 MPa applied to the specimen during the fatigue cycle will generate intrusion stresses higher than these "average" values, however, but there was no evidence that these caused cracking of the alumina intrusions.

It can be surmised from the cumulative probability plots of Figure 5 and from Figure 8 that intrusion stresses more than ~500 MPa would be required to demonstrate with statistical significance that enhanced intergranular penetration was taking place. Such stresses could not be maintained in most alloys in which creep and plastic relaxation within the alloy matrix would occur. This may explain why experimental evidence for the SAGBO effect has been elusive and inconsistent. Recent generations of polycrystalline superalloys of high strength can be expected to demonstrate a SAGBO effect however.

6. CONCLUSIONS

- Double edge notched specimens of the Ni-based superalloy RR1000 have been subjected to 1-1-1-1 fatigue tests with R=0 at 750°C in air for ~ 10^5 cycles (111 hours)

at a peak section stress of 900 MPa. The specimens ran out with no detectable fracture damage or oxide cracking.

- The oxide that formed during the test consisted of a surface layer of chromia, outcroppings of rutile and intergranular intrusions of alumina underlying the chromia layer. This oxide morphology is characteristic of this type of Ni-based superalloy. No effect of the applied axial stress on chromia thickness was detected by comparing the regions of maximum stress (base of the notches) with unstressed regions. By contrast, a significant increase in the depth of intergranular penetrations was found in the highly-stressed regions at the base of the notches. The increase in depth was approximately a factor 2 over that found in unstressed regions. This is taken to be evidence of Stress Aided Grain Boundary Oxidation (SAGBO).
- A model for the SAGBO process has been developed in which the axial tensile stress within the alumina intrusion at its tip increases the oxygen vacancy concentration there. As a result, the vacancy diffusion flux along the intrusion from its tip will increase and lead to an enhanced growth rate of the intrusion.
- Quantitative development of this model has been undertaken, albeit with a number of simplifying assumptions. Nevertheless, the results are encouraging and indicate that the observed increased intrusion depth can occur at a tip stress of around 1 GPa within the intrusion. This is considered plausible in this high-strength alloy but it implies that a SAGBO effect would be difficult to demonstrate experimentally in weaker alloys in which such large stresses could not be sustained.

7. ACKNOWLEDGEMENTS

Thanks are given to the centre for electron microscopy at the University of Birmingham for the provision of technical equipment and assistance that this work heavily relied upon. The authors also thank Rolls-Royce plc who provided the test material as well as contributing financially to this work along with the UK's Engineering and Physical Sciences Research Council through grant number EP/H022309/1.

Appendix

Calculation of the Volume Increase on Alumina Formation in RR1000

The volume change on alumina formation is usually expressed by the Pilling Bedworth Ratio (PBR), conventionally defined as the ratio of the volume of alumina formed to the volume of metal consumed in its formation. The evaluation of the PBR for pure metals is straightforward and can be obtained from molar volumes and the respective densities of the two phases. For the case of alumina formed from pure Al the PBR is 1.28. The situation is less clear when Al is a constituent of an alloy as in the present case. The current consensus is that the molar quantities used should be those for the alloy, rather than the element, and that is the route taken here.

The effective volume, Ω_m, of an Al atom in the alloy can then be calculated from molar volumes as:

$$\Omega_m = \left(\frac{M_m}{\rho_m N_A} \right) \tag{A1}$$

Here ρ_m is the alloy density, N_A is Avogadro's number (6.022×10^{23}) and M_m is the average molecular mass of the alloy calculated by:

$$M_m = \Sigma_i \left(f_i M_i \right) \tag{A2}$$

Where f_i is the atom fraction of element i, given in Table A1, M_i is its atomic mass, and the summation applies to all elements given in that table.

Table A1 - Nominal composition of RR1000 in atom fraction

Ni	Co	Cr	Mo	Ti	Al	Ta	Hf	Zr	C	B
0.5083 (bal.)	0.179	0.165	0.030	0.043	0.064	0.0063	0.0016	0.0004	0.0014	0.001

Using this approach, the mean atomic mass, M_m, is obtained as 57.11 g. Substituting this value into equation A1 with ρ_m= 8.54 g.cm^{-3} yields a value for the average atomic volume, Ω_m, for

RR1000 of 1.11×10^{-23} cm^3 (1.11×10^{-29} m^3). This is similar to the atomic volume of Ni of 1.10×10^{-23} cm^3.

The effective Pilling-Bedworth ratio, Φ, for internal alumina formation in the alloy, is calculated using this value of the atomic volume for RR1000 on the basis that this is the effective volume occupied by an Al atom within the alloy. The molecular volume of alumina, $\Omega_{Al_2O_3}$, is then obtained in an analogous manner to equation A1:

$$\Omega_{Al_2O_3} = \left(\frac{M_{Al_2O_3}}{\rho_{Al_2O_3} N_A} \right) \tag{A3}$$

Where $M_{Al_2O_3}$ is the molecular mass of alumina (101.96 g) and $\rho_{Al_2O_3}$ is its density (3.95 $g.cm^{-3}$). The molecular volume is obtained as 4.29×10^{-23} cm^3 (4.29×10^{-29} m^3). Noting that two Al atoms are necessary to form alumina, the effective Pilling-Bedworth ratio is finally obtained as:

$$\Phi = \left(\frac{\Omega_{Al_2O_3}}{2\,\Omega_m} \right) = 1.93 \tag{A4}$$

and the volumetric expansion on the formation of a molecule of alumina is 0.93 (93%). The volume term Ω_A, defined in the text by equation (3), is:

$$\Omega_A = \Omega_{Al2O3} - 2\Omega_{Al} = 2.07 \times 10^{-29}\ m^3 \tag{A5}$$

REFERENCES

1. L. Berchtold, M. Welker, H.G. Sockel, Influence of creep deformation on the formation of the oxide layer on the high temperature alloy Ni20Cr, Werks Korr 37 (1986)145-149.
2. M.M. Nagl, W.T. Evans, D.J. Hall, S.R.J. Saunders, An in situ investigation of the tensile failure of oxide scales, Oxid Met 42 (1994) 431-449.
3. I. Küppenbender, M. Schütze, The deformation behaviour of NiO scales on Ni in argon and air at temperatures from 20 to 800°C with respect to the relief of growth stresses, Oxid Met 42 (1994) 109-144.
4. C. Bruns, M. Schütze, Investigation of the mechanical properties of oxide scales on nickel and TiAl, Oxid Met 55 (2001) 35-68.
5. S. Osgerby, K. Berriche-Bouhanek, H.E. Evans, Tensile cracking of a chromia layer on a stainless steel during thermal cycling with hold periods, Mater Sci Eng A 412 (2005) 182-190.
6. V. Maurel, M. Harvey, L. Rémy, Aluminium oxide spallation on NiAl coating induced by compression, Surf Coat Techn 205 (2011) 3158-3166.
7. H.E. Evans, Cracking and spalling of protective oxide layers, Mater Sci Eng A 120 (1989) 139-146.
8. G. Moulin, P. Aravalo, A. Salleo, Influence of external mechanical loadings (creep, fatigue) on oxygen diffusion during nickel oxidation, Oxid Met 45 (1996) 153-181.
9. G. Calvarin-Amari, R. Molins, A.M. Huntz, Effect of the application of a mechanical load on the oxide-layer microstructure and on the oxidation mechanism of Ni-20Cr foils, Oxid Met 54 (2000) 399-426.
10. R. Duan, A. Jalowicka, K. Unocic, B.A. Pint, P. Huczkowski, A. Chyrkin, D. Grüner, R. Pillai, W.J. Quadakkers, Predicting oxidation-limited lifetime of thin-walled components of NiCrW alloy 230, Oxid Met 87 (2017) 11-38.
11. C. Roy, B. Burgess, A study of the stresses generated in zirconia films during the oxidation of zirconium alloys, Oxid Met 2 (1970) 235-261.
12. V.K. Tolpygo, J.R. Dryden, D.R. Clarke, Determination of the growth stress and strain in α-Al_2O_3 scales during the oxidation of Fe-22Cr-4.8Al-0.3Y alloy, Acta Mater 46 (1998) 927-937.
13. C. Sarioglu, E. Schumann, J.R. Blachere, F.S. Pettit, G.H. Meier, X-ray determination of stresses in alumina scales on high temperature alloys, Mater High Temp 17 (2000) 109-115.
14. H.E. Evans, D.J. Norfolk, T. Swan, Perturbation of parabolic kinetics resulting from the accumulation of stress in protective oxide layers, J Electrochem Soc 125 (1978) 1180-1185.
15. A.M. Limarga, D.S. Wilkinson, Modeling the interaction between creep deformation and scale growth process, Acta Mater 55 (2007) 189-201.
16. A.M. Limarga, D.S. Wilkinson, Creep-driven nitride scale growth in γ-TiAl, Acta Mater 55 (2007) 251-260.

17. H.E. Evans, Stress effects in high temperature oxidation of metals, Int Mater Rev 40 (1995) 1-40.

18. C.C. Dollins, M. Jursich, A model for the oxidation of zirconium-based alloys, J Nucl Mater 113 (1983) 19-24.

19. G. Zumpicchiat, S. Pascal, M. Tupin, C. Berdin-Méric, Finite element modelling of the oxidation kinetics of zircaloy-4 with a controlled metal-oxide interface and the influence of growth stress, Corr Sci 100 (2015) 209-221.

20. Y. Suo, S. Shen, General approach on chemistry and stress coupling effects during oxidation, J Appl Phys 114 (2013) 164905-1-164905-6

21. X. Dong, X. Fang, X. Feng, K.-C. Hwang, Diffusion and stress coupling effect during oxidation at high temperature, J Am Ceram Soc 96 (2013) 44-46.

22. X. Dong, X. Feng, K.-C. Hwang, Stress-diffusion interaction during oxidation at high temperature, Chem Phys Lett 614 (2014) 95-98.

23. X. Dong, X. Fang, X. Feng, X. Sun, Oxidation at high temperature under three-point bending considering stress-diffusion coupling effects, Oxid Met 86 (2016) 125-133.

24. A.M. Emsley, M.P. Hill, Intergranular oxidation of silicon in 20Cr-25Ni niobium-stabilised stainless steel at 1140-1230 K, Oxid Met 34 (1990) 351-360.

25. J.H. Chen, P.M. Rogers, J.A. Little, Oxidation behaviour of several chromia-forming commercial nickel-base superalloys, Oxid Met 47 (1997) 381-410.

26. C.K. Sudbrack, S.L. Draper, T.T. Gorman, J. Telesman, T.P. Gabb, D.R. Hull, Oxidation and the effects of high temperature exposures on notched fatigue life of an advanced powder metallurgy disk superalloy in "12th International Symposium on Superalloys", TMS, (2012) 863-872.

27. S. Cruchley, M.P. Taylor, H.E. Evans, M.C. Hardy, D.J. Child, Characterisation of subsurface oxidation damage in Ni based superalloy, RR1000, Mater Sci Tech 30 (2014) 1884-1889.

28. S. Cruchley, H.Y. Li, H.E. Evans, P. Bowen, D.J. Child, M.C. Hardy, The role of oxidation damage in fatigue crack initiation of an advanced Ni-based superalloy, Int J Fatigue 81 (2015) 265-274.

29. D.F. Smith, E.F. Clatworthy, D.G. Tipton, W.L. Mankins, Improving the notch-rupture strength of low-expansion superalloys, "Superalloys 1980", Proc. 4th Int. Conf. on Superalloys, Seven Springs, Pa., pp. 521-530, ASM, Metals Park, OH, (1980).

30. R.R. Stephens, L. Grabowski, D.W. Hoeppner, The effect of temperature on the behaviour of short fatigue cracks in waspaloy using an in situ SEM fatigue apparatus, Int. J. Fatigue 15 (1993) 273-282.

31. F. Gabrielli, R.M. Pelloux, Effect of Environment on fatigue and creep crack growth in Inconel X-750 at elevated temperature, Metall Trans A 13 (1982) 1083-1090.

32. V. Lupinc, G. Onofrio, The effect of creep and oxidation on high-temperature fatigue crack propagation in <001>-loaded CMSX-2 superalloy single crystals, Mater Sci Eng A 202 (1995) 76-83.

33. K.R. Bain, R.M. Pelloux, Effect of environment on creep crack growth in PM/HIP Rene-95, Metall Trans A 15 (1984) 381-388.

34. H.H. Smith, D.J. Michel, Effect of environment on fatigue crack propagation behaviour of alloy 718 at elevated temperatures, Metall Trans A 17 (1986) 370-374.

35. L. Viskari, S. Johansson, K. Stiller, Oxygen influenced intergranular crack propagation: analysing microstructure and chemistry in the crack tip region, Mater High Temp 28 (2011) 336-341.

36. L. Viskari, M. Hörnqvist, K.L. Moore, Y. Cao, K. Stiller, Intergranular crack tip oxidation in a Ni-base superalloy, Acta Mater 61 (2013) 3630-3639.

37. C.F. Miller, G.W. Simmons, R.P. Wei, Evidence for internal oxidation during oxygen enhanced crack growth in P/M Ni-based superalloys, Scr Mater 48 (2003) 103-108.

38. J. Tong, S. Dalby, J. Byrne, M.B. Henderson, M.C. Hardy, Creep, fatigue and oxidation in crack growth in advanced nickel base superalloys, Int J Fatigue 23 (2001) 897-902.

39. D.M. Knowles, D.W. Hunt, The influence of microstructure and environment on the crack growth behaviour of powder metallurgy nickel superalloy RR1000, Metall Mater Trans A 33 (2002) 3165-3172.

40. X. Liu, B. Kang, W. Carpenter, E. Barbero, Investigation of the crack growth behaviour of Inconel 718 by high temperature moire interferometry, J Mater Sci 39 (2004) 1967-1973.

41. H. Ghonem, T. Nicholas, A. Pineau, Elevated temperature fatigue crack growth in alloy 718 – part II: effects of environmental and material variables, Fatigue Fract Eng Mater Struct 16 (1993) 577-590.

42. J. Gayda, R.V. Miner, Fatigue crack initiation and propagation in several nickel-base superalloys at 650°C, Int J Fatigue 5 (1983) 135-143.

43. R.H. Bricknell, D.A. Woodford, The embrittlement of nickel following high temperature air exposure, Metall Trans A 12 (1981) 425-433.

44. H.S. Kitaguchi, H.Y. Li, H.E. Evans, R.G. Ding, I.P. Jones, G. Baxter, P. Bowen, Oxidation ahead of a crack tip in an advanced Ni-based superalloy, Acta Mater 61 (2013) 1968-1981.

45. C.J. McMahon, L.F. Coffin Jr., Mechanisms of damage and fracture in high-temperature, low-cycle fatigue of a cast nickel-based superalloy, Metall Trans 1 (1970) 3443-3450.

46. E. Andrieu, R. Molins, H. Ghonem, A. Pineau, Intergranular crack tip oxidation mechanism in a nickel-based superalloy, Mater Sci Eng A 154 (1992) 21-28.

47. A.A.N. Nemeth, D.J. Crudden, D.E.J. Armstrong, D.M. Collins, K. Li, A.J. Wilkinson, C.R.M. Grovenor, R.C. Reed, Environmentally-assisted grain boundary attack as a mechanism of embrittlement in a nickel-based superalloy, Acta Mater 126 (2017) 361-371.

48. H.Y. Li, J.F. Sun, M.C. Hardy, H.E. Evans, S.J. Williams, T.J.A. Doel, P. Bowen, Effects of microstructure on high temperature dwell fatigue crack growth in a coarse grain PM nickel based auperalloy, Acta Mater 90 (2015) 355-369.

49. H.S. Kitaguchi, M.P. Moody, H.Y. Li, H.E. Evans, M.C. Hardy, S. Lozano-Perez, An atom probe tomography study of the oxide-metal interface of an oxide intrusion ahead of a crack in a polycrystalline Ni-based superalloy, Scr Mater 97 (2015) 41-44.

50. M. Hörnqvist, L. Viskari, K.L. Moore, K. Stiller, High-temperature crack growth in a Ni-base superalloy during sustained load, Mater Sci Eng A 609 (2014) 131-140.

51. F.H. Stott, Y. Shida, D.P. Whittle, G.C. Wood, B.D. Bastow, The morphological and structural development of internal oxides in nickel-aluminium alloys at high temperatures, Oxid Met 18 (1982) 127-146.

52. L. Ma, K.-M. Chang, Identification of SAGBO-induced damage zone ahead of crack tip to characterise sustained loading crack growth in alloy 783, Scr Mater 48 (2003) 1271-1276.

53. A. Selvig, X. Huang, M. Hildebrand, D. Stek, Investigation of stress assisted grain boundary oxidation cracking in MAR-M002 high pressure turbine blades, J Eng Gas Turbines Power 133 (2011), 082101/1-082101/8

54. G. Bertali, F. Scenini, M.G. Burke, The effect of residual stress on the preferential intergranular oxidation of alloy 600, Corr Sci 111 (2016) 494-507.

55. H.E. Evans, H.Y. Li, P. Bowen, A mechanism for stress-aided grain boundary oxidation ahead of cracks, Scr Mater 69 (2013) 179-182.

56. S. Cruchley, M.P. Taylor, R. Ding, H.E. Evans, D.J. Child, M.C. Hardy, Comparison of chromia growth kinetics in a Ni-based superalloy, with and without shot-peening, Corr Sci 100 (2015) 242-252.

57. P. Hancock, J.R. Nicholls, K. Mahmood, The influence of imposed strain rate on fracture of surface oxides, Corr Sci 35, (1993), 979-987.

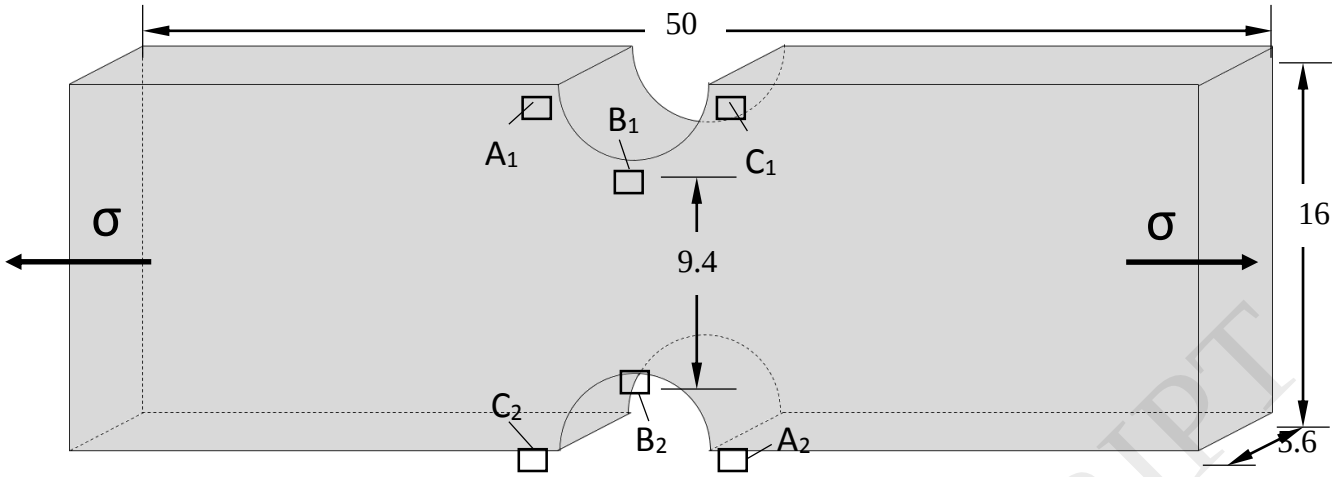

Figure 1 – A diagram showing dimensions of the DEN cyclic tensile stress specimen and the locations (A, B, C) at which detailed metallographic examination was undertaken. All dimensions in millimetres. Loading direction is indicated by arrows labelled with σ.

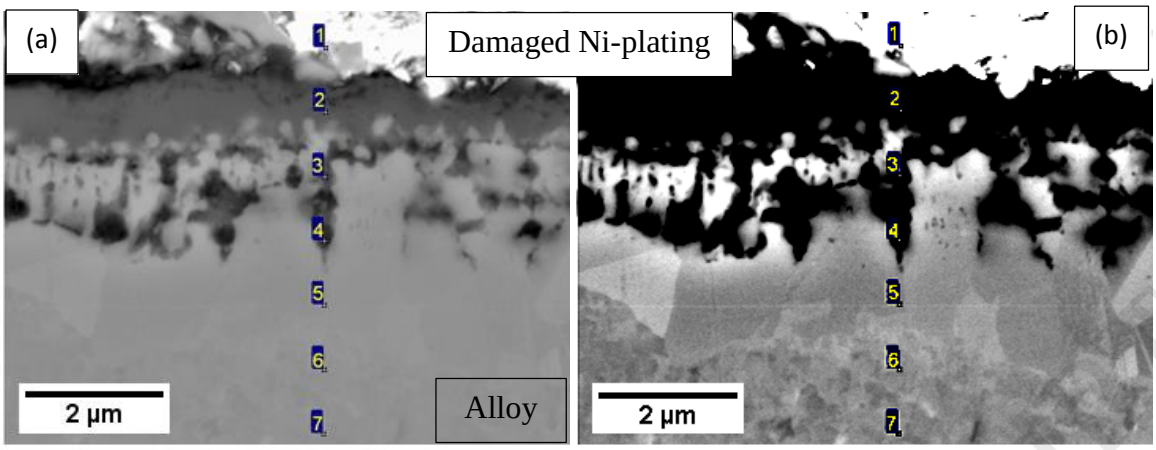

Figure 2: BSE images of the same region with differing contrast settings (a) showing the typical external oxide and subscale intrusion oxidation behaviour, and the location of a set of EDS point scans down one such intrusion, and (b) emphasising the recrystallization of the alloy just beneath the oxide.

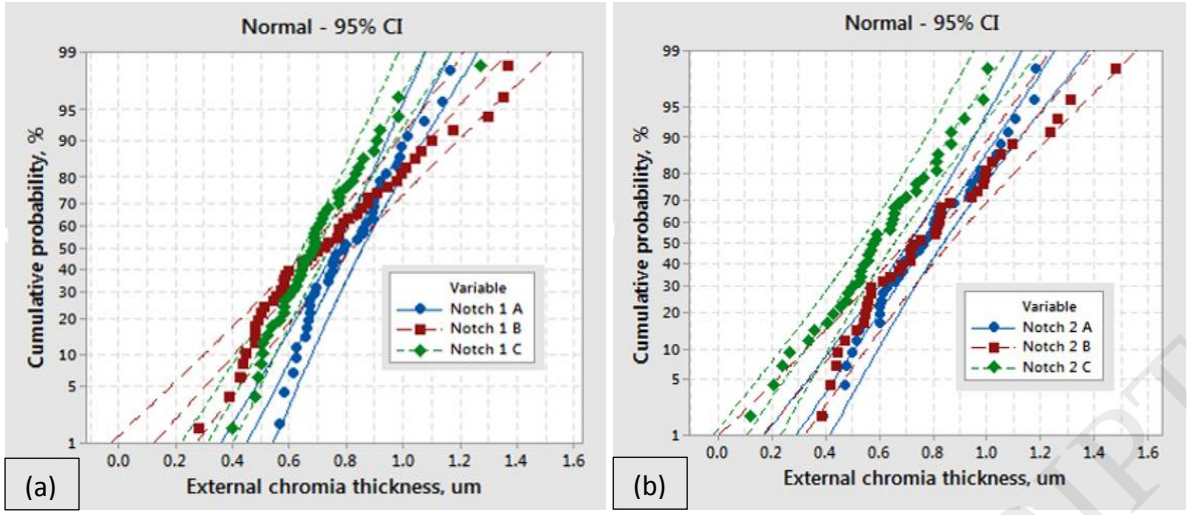

Figure 3: Cumulative probability plots for the chromia layer thickness for each of the sampling locations for (a) Notch 1 and (b) Notch 2. The lines are fitted to the data and show the 95% confidence limits.

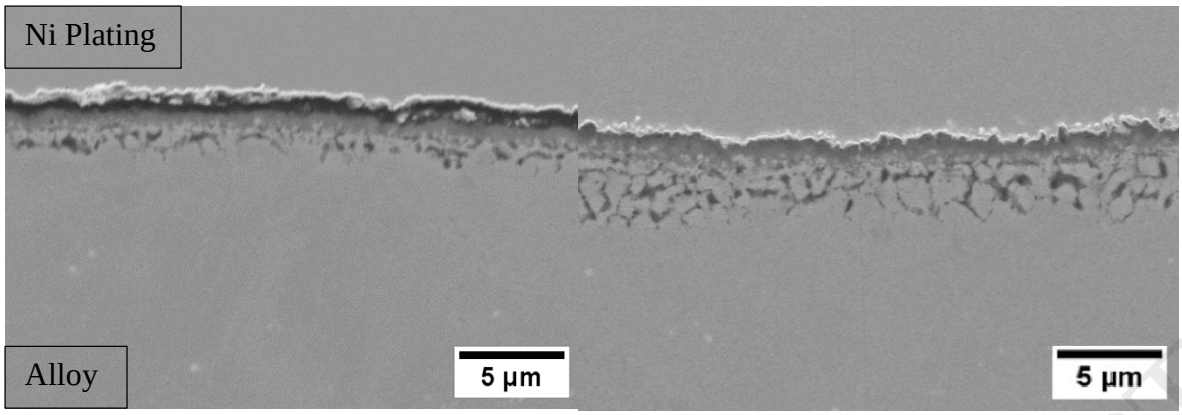

Location C, Notch 1 Location B, Notch 1

(a)

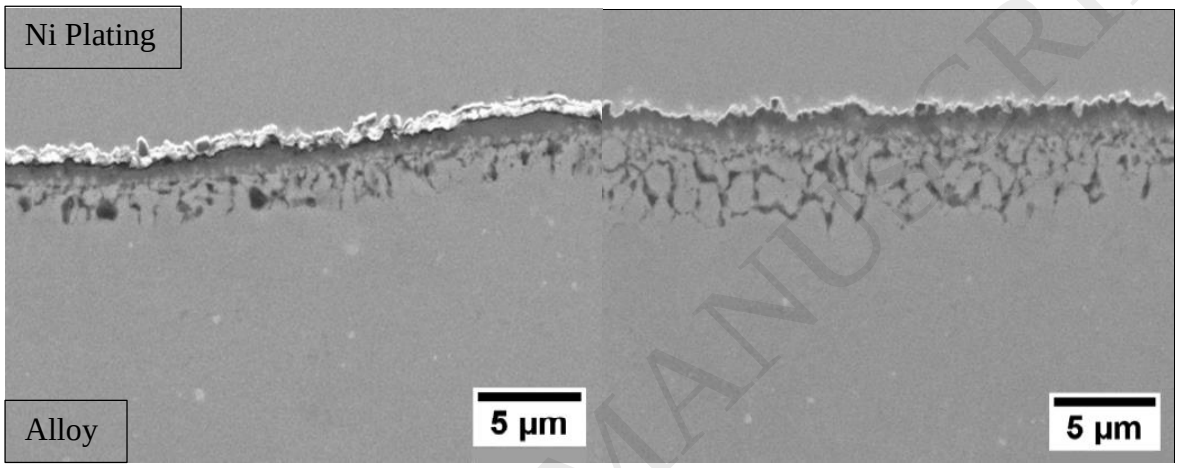

Location A, Notch 2 Location B, Notch 2

(b)

Figure 4: A comparison of the oxide morphology formed at Locations A/C (negligible applied stress) with that at Location B (maximum applied stress) for (a) Notch 1 and (b) Notch 2.

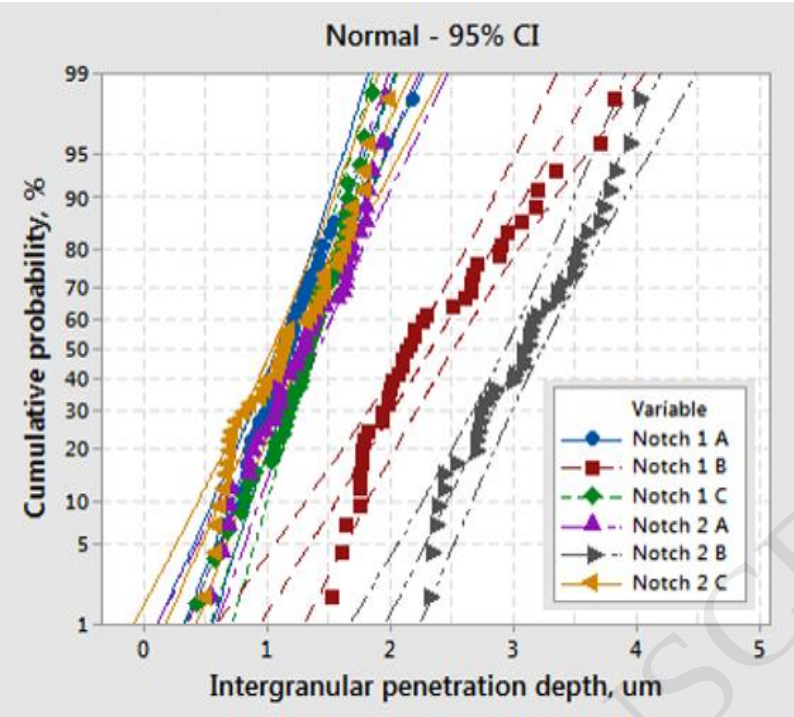

Figure 5: Cumulative probability plots of the depth of alumina intergranular intrusions for each of the sampling locations for Notch 1 and Notch 2. The lines are fitted to the data and show the 95% confidence intervals.

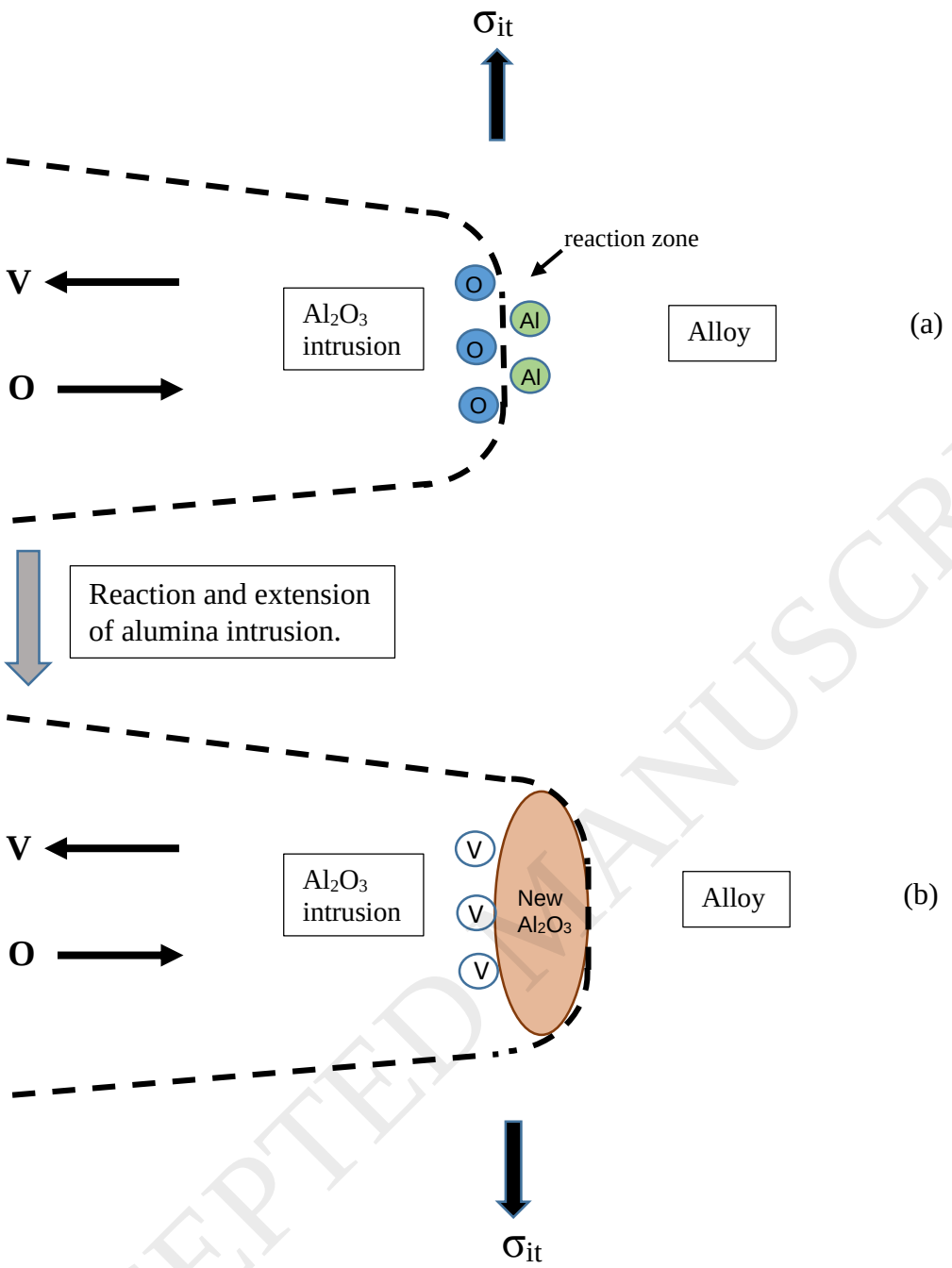

Figure 6: A schematic representation of the intrusion tip, (a) prior to further reaction and (b) after reaction showing the creation of oxygen vacancies.

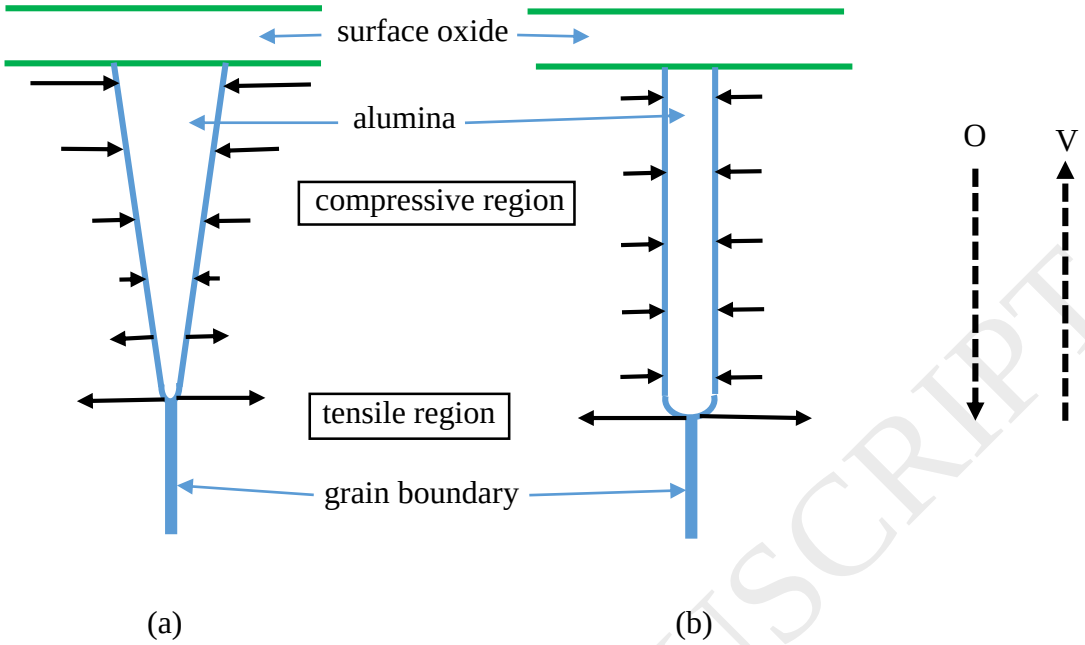

Figure 7: Stress distribution orthogonal to the plane of the grain boundary for (a) a wedge-shaped intrusion and (b) an intrusion of constant width. The directions of flow of oxygen ions and oxygen vacancies are shown by the broken lines on the right-hand side of the figure.

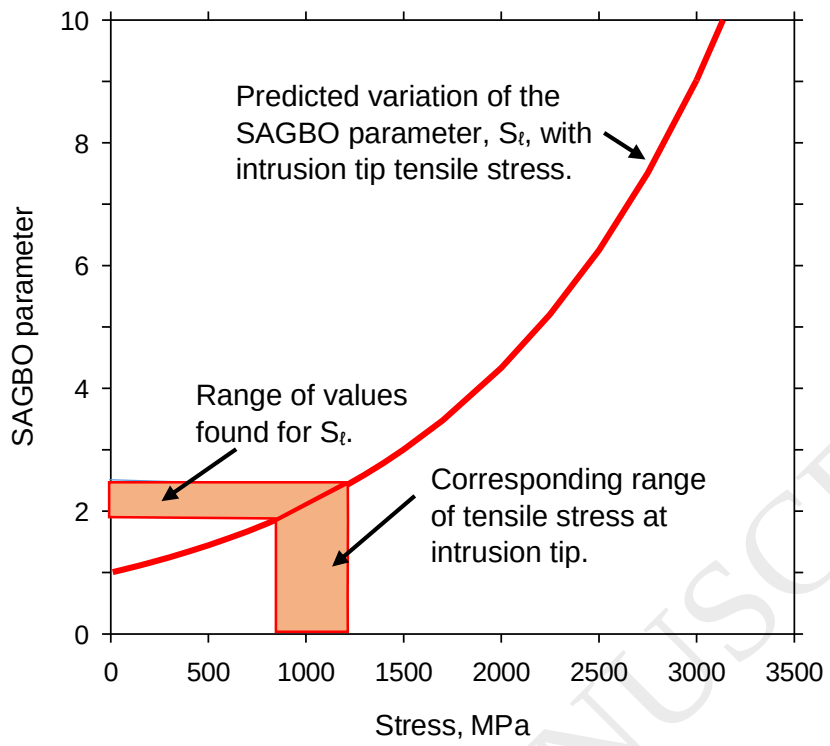

Figure 8: The predicted variation, from equation 14, of the SAGBO parameter, S_ℓ, with the tensile stress within the intrusion at its tip. The shaded regions show the range found for S_ℓ, in the present work and the corresponding stresses.

Table 1: Nominal composition of RR1000 in both weight and atomic %

	Ni	Co	Cr	Mo	Ti	Al	Ta	Hf	Zr	C	B
Weight %	bal.	18.5	15.0	5.0	3.6	3.0	2.0	0.5	0.06	0.02	0.03
Atomic %	bal.	17.9	16.5	3.0	4.3	6.4	0.6	0.2	0.04	0.14	0.10

Table 2: EDS results for each element of the alloy composition at each point indicated in Figure 2. All results are given in wt.% with average errors but the values are indicative only for the narrow oxide intrusions because of the associated large matrix capture volume.

Point	O	Ni	Co	Cr	Ti	Al	Mo	Ta	Hf
1	9.4	69.6	2.2	7.4	3.4	0.7	4.7	2.4	0.2
2	28.3	16.4	3.5	37.9	8.9	1.4	1.3	2.1	0.2
3	12.4	38.6	15.5	11.8	2.6	8.1	5.8	3.3	2.0
4	8.2	46.6	18.2	8.5	1.1	9.5	6.2	0.8	1.0
5	0.1	59.9	20.2	9.7	0.8	1.0	6.4	1.6	0.2
6	-	58.8	15.9	9.2	4.1	3.2	4.4	2.8	1.5
7	-	51.6	19.1	14.4	3.4	2.8	6.0	2.3	0.4
Average errors for points 2-7	0.5	0.6	0.3	0.3	0.2	0.2	0.5	0.4	0.6

Table A2 - Nominal composition of RR1000 in atom fraction

Ni	Co	Cr	Mo	Ti	Al	Ta	Hf	Zr	C	B
0.5083 (bal.)	0.179	0.165	0.030	0.043	0.064	0.0063	0.0016	0.0004	0.0014	0.001